

# Critical Behavior of a Chiral Condensate with a Meron Cluster Algorithm

Shailesh Chandrasekharan and James C. Osborn,<sup>a</sup>

<sup>a</sup>Department of Physics, Duke University, Durham, NC 27708-0305, USA

A new meron cluster algorithm is constructed to study the finite temperature critical behavior of the chiral condensate in a  $(3+1)$  dimensional model of interacting staggered fermions. Using finite size scaling analysis the infinite volume condensate is shown to be consistent with the behavior of the form  $(T_c - T)^{0.314(7)}$  for temperatures less than the critical temperature and  $m^{1.487(10)}$  at the critical temperature confirming that the critical behavior belongs to the 3-d Ising universality class within one to two sigma deviation. The new method, along with improvements in the implementation of the algorithm, allows the determination of the critical temperature  $T_c$  more accurately than was possible in a previous study.

## 1. Motivation

The construction of Monte Carlo algorithms to solve problems in many body quantum mechanics involving fermions is notoriously difficult. This difficulty is reflected in our inability to perform precise quantitative calculations in strongly interacting fermionic models which are necessary to understand a variety of phenomena including high temperature superconductivity and the physics of strongly interacting matter. The essential problem arises due to the Pauli principle which can produce negative Boltzmann weights when the quantum partition function is rewritten as a path integral in a convenient basis. As a result, the probability distribution that should be used for importance sampling is unclear.

The conventional approach to problems involving fermions is to integrate them out in favor of a fermion determinant. In cases where this determinant is positive it is often possible to use known sampling methods for a bosonic problem to devise an algorithm [1-4]. Some of these methods are inexact since they involve discretization of a differential equation and require some care and study before they can be applied to a new problem. Others can suffer from truncation errors that approximate the original partition function. Worst of all, these algorithms suffer from the usual problems of critical slowing which makes it difficult to study phase transitions using them.

The study of phase transitions, especially in the context of fermionic models, is of interest in a variety of fields. In condensed matter physics strong correlations between electrons can lead to many interesting critical effects like high  $T_c$  superconductivity [5] and quantum phase transitions [6]. In high energy physics, existence of new phases and fixed points have been predicted [7-9] which may lead to novel formulations of quantum field theories beyond

perturbation theory. Additionally, exotic phases arise in dense nuclear matter due to strong interactions among quarks [10].

Since fermions acquire a screening mass on the order of the temperature  $T$ , one expects that the finite temperature critical behavior close to a second order phase transition in a  $(d+1)$  dimensional theory is governed by a  $d$  dimensional low energy effective theory that is purely bosonic [11]. A few years ago, this conventional wisdom was questioned based on a large  $N$  calculation [12] in a Gross-Neveu model. It was shown that the finite temperature phase transition in the  $(2+1)$  dimensional model reproduced mean field exponents instead of the expected 2-d Ising exponents. This claim was later backed by numerical evidence [13] using the hybrid Monte Carlo algorithm. Although, the reason for the unexpected critical behavior was later attributed to the narrowness of the Ginsburg region in the large  $N$  limit [14], the numerical evidence provided to substantiate the earlier claims remains disturbing and perhaps shows the inadequacy of the numerical methods used. Recently, the chiral transition in two flavor QCD with an additional four-fermion interaction was studied using the hybrid molecular dynamics algorithm which showed evidence for non-mean field critical exponents [15]. However, again the expectations based on simple dimensional reduction were not observed, instead the data appeared to be consistent with tricritical behavior.

The inability to provide conclusive answers to questions related to the critical behavior in fermionic theories is closely related to the lack of efficient fermion algorithms. The fermion cluster algorithms, recently proposed in [16,17], provide a novel approach to the problem. The new method, referred to as the meron cluster algorithm, uses well known quantum cluster algorithm techniques [18]

to solve the fermion sign problem completely. The first applications of the meron algorithm emerged last year when it was used to study the critical behavior in a relativistic system of interacting staggered fermions with a discrete chiral symmetry [19,20]. The results indicated that the symmetry is broken by the ground state but is restored by thermal fluctuations at high temperatures. However, in order to avoid the complications that arise in the algorithm due to the addition of a mass term, the previous study focused on massless fermions. Since the chiral condensate vanishes in this case the scaling of the chiral susceptibility with the volume was used to find the critical temperature and the critical exponents [21].

In this article a new meron algorithm is proposed and applied to study the staggered fermion model in the presence of the mass term<sup>1</sup>. This makes it possible to study the critical behavior of the chiral condensate. The main result of the article is that in (3+1) dimensions the chiral condensate behaves like  $\langle \bar{\psi} \psi \rangle = A(T_c - T)$  just below  $T_c$  with  $\beta = 0.314(7)$  and vanishes for higher temperatures. The corresponding exponent in the 3-d Ising model is known to be 0.32648(18). As a bonus the critical temperature is also determined more accurately than previous studies. Furthermore at  $T_c$  the mass dependence of the condensate also behaves as expected,  $\langle \bar{\psi} \psi \rangle = B m^{-1}$ , where  $\beta = 4.87(10)$  as compared to 4.7893(22) of the Ising model. Conventional fermionic algorithms have never been able to confirm the predictions of universality in a strongly interacting fermionic model with such precision.

## 2. The Model

The Hamilton operator for staggered fermions hopping on a 3-d cubic spatial lattice with  $V = L^3$  sites ( $L$  even) and anti-periodic spatial boundary conditions, considered here, is given by

$$H = \sum_{x,i} h_{x,i} + m \sum_x s_x \quad (1)$$

The term

$$h_{x,i} = \frac{x_{i1}}{2} (c_x^\dagger c_{x+\hat{1}} + c_{x+\hat{1}}^\dagger c_x) + (n_x - \frac{1}{2})(n_{x+\hat{1}} - \frac{1}{2}); \quad (2)$$

ouples the fermion operators at the nearest neighbor sites  $x$  and  $x + \hat{1}$  where  $\hat{1}$  is a unit-vector in the positive  $i$ -direction and the mass term

$$s_x = (-1)^{x_1 + x_2 + x_3} (n_x - \frac{1}{2}); \quad (3)$$

is a single site operator. The fermion creation and annihilation operators  $c_x^\dagger$  and  $c_x$  satisfy the canonical anti-commutation relations and  $n_x = c_x^\dagger c_x$  is the number operator. The phase factors  $x_{i1} = 1$ ,  $x_{i2} = (-1)^{x_1}$  and

$x_{i3} = (-1)^{x_1 + x_2}$  are well known in the staggered fermion formulation [21].

This model was originally studied in the chiral limit ( $m = 0$ ) in [19]. In this limit the Hamilton operator is invariant under shifts in the  $x_3$  direction. The mass term breaks this symmetry up to shifts by an even number of lattice units, thus breaking a  $Z_2$  symmetry which can be related to a subgroup of the well known chiral symmetry of relativistic massless fermions. This symmetry is broken spontaneously at zero temperatures, while thermal fluctuations restore it at some high temperatures [19]. In this article the critical behavior near the second order transition is studied using the chiral condensate  $\langle \bar{\psi} \psi \rangle = \sum_x \langle \bar{\psi}_x \psi_x \rangle = V$  using the algorithm presented in [22] and briefly sketched here.

The construction of the path integral for the partition function is standard. First, the Hamilton operator is rewritten as  $H = H_1 + H_2 + \dots + H_6 + H_7$  with

$$H_i = \sum_{\substack{x=(x_1;x_2;x_3) \\ x_i \text{ even}}} h_{x,i} \quad H_{i+3} = \sum_{\substack{x=(x_1;x_2;x_3) \\ x_i \text{ odd}}} h_{x,i} \quad (4)$$

for  $i = 1; 2; 3$  and  $H_7 = m \sum_x s_x$ . The partition function is then approximated by

$$\text{Tr} e^{-H_1} e^{-H_7/6} e^{-H_2} e^{-H_7/6} \dots e^{-H_6} e^{-H_7/6} e^{-H_3} \quad (5)$$

where the inverse temperature has been divided into  $M$  slices such that  $M = 1/T$ . At a fixed temperature, the above approximation becomes exact in the limit  $M \rightarrow \infty$  and  $\beta \rightarrow 0$ . On the other hand for any fixed  $M$ , the approximation defines a new theory with a phase structure and critical behavior that can be identical to the  $M = \infty$  theory. For simplicity this article focuses on the theory with  $M = 4$ .

## 3. Meron Cluster Algorithm

In order to solve the model discussed in the previous section using a meron cluster algorithm, the partition function should first be written in terms of fermion occupation numbers  $n$  and bond variables  $b$  so that it can be represented by

$$Z = \sum_{\{n;b\}} \prod_x \text{Sign}[n;b] W[n;b]; \quad (6)$$

Configurations  $\{n;b\}$  live on an  $L^d = 4dM$  lattice. A typical configuration in one space and one time dimension is shown in figure 1. The shaded regions represent either the nearest neighbor interactions that arise due to terms of the form  $\exp(-h_{x,i})$  or the single site interactions due to mass terms  $\exp(-m s_x)$ . The various steps that are used to determine  $W[n;b]$  and  $\text{Sign}[n;b]$  starting from the

<sup>1</sup> Preliminary results of this work was presented in [22]

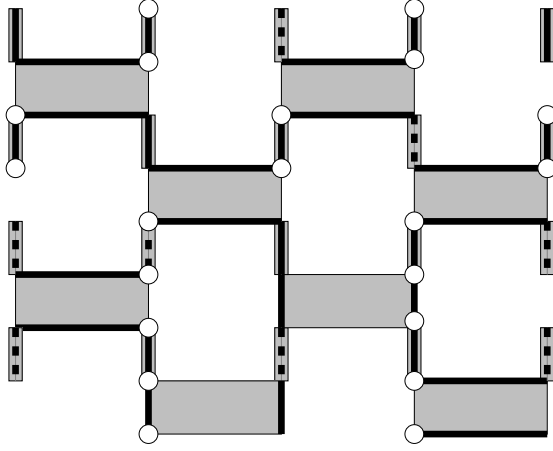


Figure 1. A configuration of fermion occupation numbers and bonds on a one dimensional periodic spatial lattice of size  $L = 4$ . Each shaded region corresponds to a transfer matrix element and has weights and signs that are shown in figure 2.

partition function (5) have been discussed in [22,19,24]. The final results can be represented as a set of simple rules.  $W[n;b]$  turns out to be a product of magnitudes of the transfer matrix elements and  $\text{Sign}[n;b]$  represents the product of their signs. The non-zero matrix elements are shown in figure 2 along with their weights. When compared to [19] the only difference is in the mass term. Assuming  $m = 0$  in (1) leads to two types of single site interactions. The one with the solid bond is always positive, and the one with the dotted bond is negative on filled even sites and empty odd sites. This extra negative sign must be included in  $\text{Sign}[n;b]$  along with sign that arises due to fermion hops, staggered fermion phase factors and anti-periodic spatial boundary conditions as discussed in [19].

Bonds connect lattice points into clusters. A flip of a cluster is defined as the change in the configuration of fermion occupation numbers at the sites belonging to the cluster, such that an occupied site is emptied and vice-versa. For a given model to be solvable using a meron cluster algorithm, the weights  $W[n;b]$  and signs  $\text{Sign}[n;b]$  must satisfy three properties under cluster flips.

1. The weight of the configuration  $W[n;b]$  must not change under the flip of any cluster.
2. The change in  $\text{Sign}[n;b]$  due to a cluster flip must be independent of the state of other clusters.

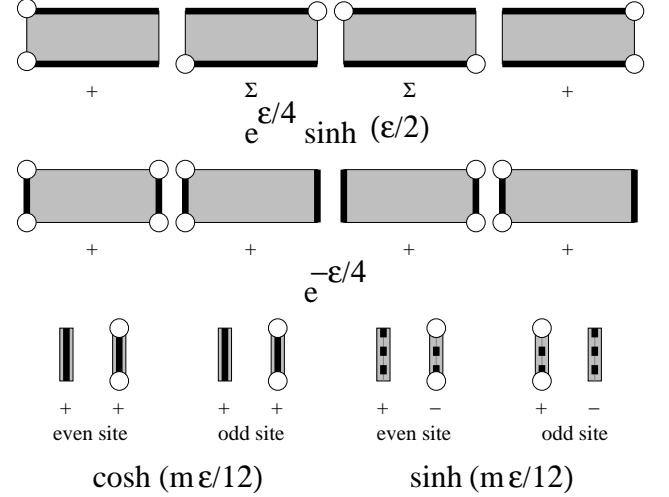


Figure 2. The magnitude and sign of the non-zero transfer matrix elements. The product of such weights over the entire lattice determine  $W[n;b]$  and  $\text{Sign}[n;b]$ . The signs get contributions from local staggered fermion phase factors and non-local factors that arise due to anti-commutation relations.

3. Starting from any configuration  $[n;b]$ , it must be possible to reach a reference configuration  $[n_{\text{ref}};b]$  by flipping clusters such that  $\text{Sign}[n_{\text{ref}};b]$  is 1.

As has been discussed in [25], the change in the sign of the configuration due to a cluster flip depends on the topology of the cluster. If we refer to the clusters whose flip changes the sign of the configuration as merons, then it is easy to classify a configuration  $[n;b]$  based on the number of meron clusters it contains. Using the above three properties it is then easy to check that the partition function gets contributions only from the zero meron sector, i.e.,

$$Z = \sum_{[n;b]} \overline{\text{Sign}[n;b]} W[n;b]; \quad (7)$$

where  $\overline{\text{Sign}[n;b]} = \frac{1}{N} \sum_{i=1}^N \text{Sign}[n;b]_i$  and  $N$  denotes the number of merons in the configuration. For the present model it is also easy to show that the chiral condensate is given by

$$\langle \bar{\psi} \psi \rangle = \frac{1}{V Z} \sum_{[n;b]} \text{Size}(C_{\text{meron}}) \sum_{i=1}^N W[n;b]; \quad (8)$$

which means that to measure the condensate one is interested only in the zero and one meron number sectors.

A typical sweep in a meron cluster algorithm consists of two steps exactly like any other cluster algorithm. Starting from a configuration the bonds are updated first based

on the weights  $W[h;b]$ . After each local bond update the meron number of the configuration can potentially change. In order not to generate more than the necessary number of merons every bond update is followed by a Metropolis decision. While measuring the chiral condensate for example one rejects all bond updates that generate more than one meron. This requires one to reanalyze the topology of clusters that are connected to the local bonds being updated. A major improvement in the implementation allows this to be done in at most  $\log(\text{Size}(C))$  steps [26]. Once all the bonds are updated it is possible to update the occupation numbers by flipping each cluster with a probability half. This algorithm produces the configuration  $[h;b]$  with weight  $(N_{i,0} + N_{i,1})W[h;b]$ . Thus, the condensate can be calculated using

$$h_i = \frac{h \text{Size}(C_{\text{meron}}) N_{i,1}}{V h_{N,0,i}}; \quad (9)$$

where  $h_{N,0,i}$  refers to a simple average over the generated configurations.

#### 4. Numerical Results

The critical behavior of the model was studied through the measurement of the chiral condensate at several values of the temperature around  $T_c$  using the algorithm discussed above. For each temperature simulations were performed on different spatial lattice sizes and at various masses. Each simulation produced  $10^6$  configurations, except for the largest lattices of sizes ranging from  $32^3$  up to  $48^3$  which contained only  $10^5$  configurations. All runs included at least ten thousand thermalization sweeps in addition to the above measurements. The autocorrelation times typically ranged from two to five sweeps. However, errors were evaluated from fluctuations in the averages of data over blocks of 1000 configurations each. For future reference we give the values of the chiral condensate on a  $32^3$  lattice obtained at  $m = 0.001$  and various temperatures in the table below.

T	$h_i$	T	$h_i$
1.0000	0.270 (20)	1.0471	0.1478 (61)
1.0152	0.228 (16)	1.0638	0.0566 (17)
1.0309	0.205 (12)	1.0870	0.0175 (04)

In order to confirm the spontaneous breaking of the  $Z_2$  chiral symmetry the condensate needs to be evaluated in the infinite volume limit followed by the chiral limit. This can be done precisely by a finite size scaling analysis. In the broken phase the theory undergoes a first order phase transition as a function of the mass at  $m = 0$  where the condensate exhibits a jump. In a large but finite volume this discontinuity is smoothed out to an analytic curve

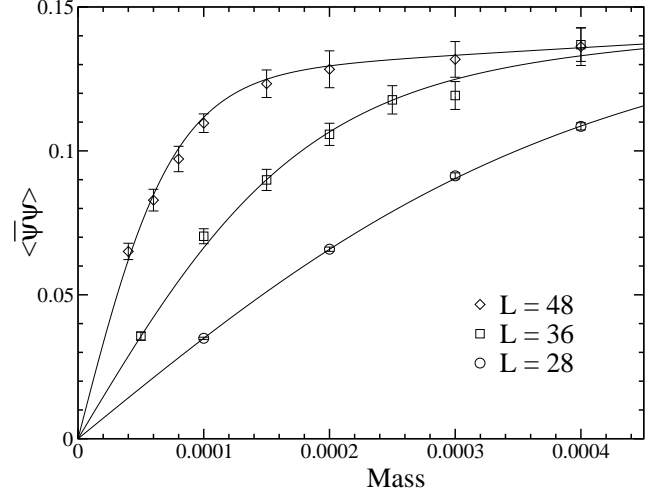


Figure 3. Chiral condensate as a function of the mass at three different lattice sizes at  $T = 1.0471$ . The data from the simulations is plotted along with the function (10) for each volume. The same values of  $\phi_0$  and  $\phi_1$  are used for all curves shown.

whose functional form is given by [27]

$$h_i = \phi_0 \tanh(m V \phi_1) + \phi_1 m; \quad (10)$$

which is valid when

$$m \phi_1 = 0; \quad (11)$$

By fitting the available data at each simulation temperature to the formula (10) it is possible to extract  $\phi_0$ , the desired limiting value of the condensate. The minimum volume necessary for the formula to work can be determined by systematically removing the smallest volume data from the fit, as required to obtain a  $\chi^2/\text{DOF}$  of about one. Finally, it is important to check if  $\phi_0$  and  $\phi_1$  obtained through the fit and the masses used are consistent with the condition (11).

The above finite size scaling analysis works exceptionally well, as can be seen from figure 3, which shows a plot of the condensate as a function of the mass at a fixed  $T = 1.0471$  for three different lattice sizes. The solid lines represent the function (10) for a fixed value of  $\phi_0$  and  $\phi_1$  obtained from a single fit to all of the shown data and more. The  $\chi^2/\text{DOF}$  for the fit is around 0.8. Since  $T = 1.0471$  is very close to the critical temperature it was necessary to go to spatial volumes as large as  $48^3$  in order to determine  $\phi_0$  with reasonable precision.

Interestingly, the above fitting procedure failed to yield an acceptable chi-squared for data above a certain temperature. This was essentially due to the fact that it was impossible to find a small enough mass to ensure that the

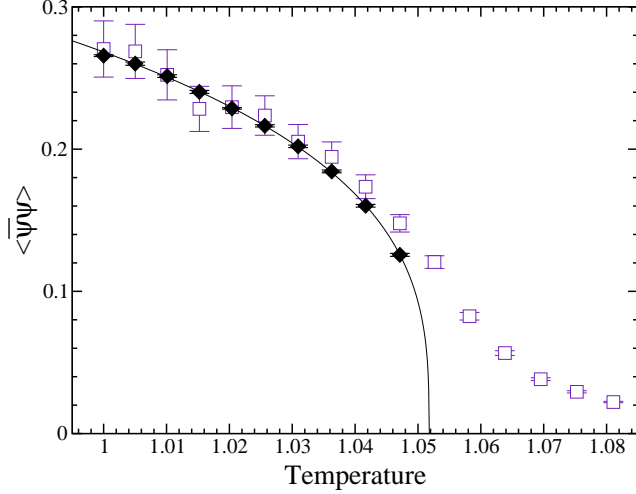


Figure 4. Chiral condensate versus temperature. The open squares are results for  $L = 32$  and  $m = 0.001$ . The filled diamonds are the extrapolation to the infinite volume limit and the chiral limit. The solid line is a plot of  $A(1.0518 - T)^{0.314}$  obtained from a fit of the extrapolated points.

condition (11) was satisfied. Removing the larger mass data resulted in a smaller  $\chi_0$  which in turn lowered the bound in (11). This observation is consistent with a vanishing condensate in the chiral limit for higher temperatures.

The non-zero values of  $\chi_0$  extracted from the fits at different temperatures are shown in figure 4. The solid line represents a fit to the expected form  $A(T_c - T)$  using the data for temperatures between 1.0050 and 1.0471. The  $\chi^2/\text{D.O.F.}$  for the fit was 0.4. The critical exponent was found to be 0.314(7) which is consistent with the measured value of 0.32648(18) in the Ising model [28] within two sigma. The fit also determines the critical temperature very accurately to be  $T_c = 1.0518(3)$  which agrees with the previously obtained result [19] within errors. The data for  $L = 32$  and  $m = 0.001$  is shown for comparison and to demonstrate the necessity of using the infinite size scaling formula (10) to extract the infinite volume chiral limit. Furthermore, the errors on  $\chi_0$  are typically much smaller than those for any single data point due to the constraints that arise from fitting over a wide range of masses and volumes.

At  $T_c$  the finite size scaling behavior of the condensate as a function of the mass is very different from (10) and can be shown to be of the form

$$\chi_0 = L^{y_m} f(L^{y_m} m) \quad (12)$$

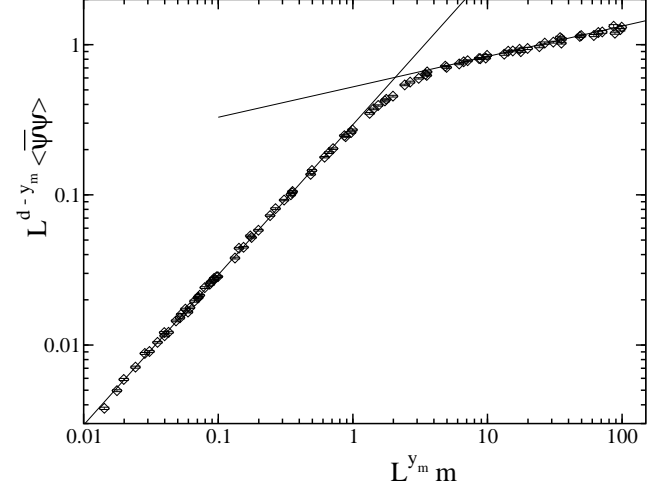


Figure 5. Log-log plot of  $L^{d-y_m} \chi_0$  versus  $L^{y_m} m$  which describes the scaling function given in (12). The value of  $y_m$  used is obtained from a fit to the small  $x$  data as explained in the text. The solid lines are fits to (13) for small  $x$  and (14) for large  $x$  data.

using renormalization group arguments that are valid close to a second order phase transition. For any  $Z_2$  phase transition the function  $f(x)$  is universal and depends only on the lattice geometry, boundary conditions etc., and not on the type of lattice, irrelevant operators and such. The exponent  $y_m$  is hence universal. The behavior of  $f(x)$  is known in the two limits:

$$f(x) \sim x^{1/2} \quad \text{for } x \rightarrow 0; \quad (13)$$

$$f(x) \sim x^{1/4} \quad \text{for } x \rightarrow \infty; \quad (14)$$

where  $1/2 = (d - y_m)/2 = y_m$ .

Based on the estimate of  $T_c$  obtained above, additional simulations at  $T = 1.0518$  were performed to confirm this critical behavior as a function of the mass. Using the data with  $L = 8$  and  $L^{y_m} m \leq 0.1$ , the chiral condensate is fit to the form

$$\chi_0 = f_0 L^{2y_m} \chi_m \quad (15)$$

based on the expectation from (13). Using this value of  $y_m$ , we can calculate

$$\chi_m = 4.87(10) \quad (16)$$

which compares favorably with the known value for the Ising model of 4.7893(22) [28]. Using the fitted value of  $y_m$ , the quantity  $L^{d-y_m} \chi_0$  is plotted in figure 5 for all available data as a function of  $L^{y_m} m$ . Clearly the data collapses onto a single curve within errors, as expected from (12). To confirm this picture the data in figure 5

with  $L = 12$  and  $10 < L^y m < 90$  is fit to the form (14). This yields the value  $\beta = 4.89(19)$  which agrees with the earlier determination and further demonstrates that the critical behavior in the present model is consistent with the 3-d Ising universality class.

## 5. Conclusions

The meron cluster algorithm has allowed a direct simulation of a strongly interacting fermionic theory in the vicinity of a  $Z_2$  chiral phase transition on lattices with spatial volumes of up to  $48^3$  using common workstation computers. The scaling behavior near the critical point, as a function of both the temperature and mass, was determined within errors of about 2% and the results are consistent with a second order phase transition. Allowing for 1-2 sigma deviations the universality class of the transition matches with that of the 3-d Ising model. This result strongly supports the scenario where a fermionic theory in  $d+1$  dimensions undergoes a dimensional reduction to be described by a  $d$  dimensional bosonic theory in the critical region. Comparing similar results with the hybrid Monte Carlo algorithm, the meron algorithm provides great improvement over such methods.

## Acknowledgement

We would like to thank Uwe Wiese for many useful discussions. This work was supported in part by a grant from the US Department of Energy, Office of Energy Research (DE-FG 02-96ER 40945). The computations were performed on Brahma, a Pentium based Beowulf cluster constructed using computers donated generously by the Intel Corporation and located in the physics department at Duke University.

## REFERENCES

1. S. Duane and J. Kogut, Phys. Rev. Lett. 55, 2774 (1985); Nucl. Phys. B 275, 398 (1986).
2. A. M. Horowitz, Phys. Lett. 156B, 89 (1985); Nucl. Phys. B 280, 510 (1987); Phys. Lett. 268B, 247 (1991).
3. S. R. White et. al., Phys. Rev. B 38, 11695 (1988); Phys. Rev. B 40, 506 (1989);
4. M. Luscher, Nucl. Phys. B 418, 637 (1994).
5. P. W. Anderson, Science 235, (1987) 1196.
6. S. Sondhi, S. Girvin, J. Carini and D. Shahar, Rev. Mod. Phys. 69, 315 (1997);
7. J. Kogut, E. Dagotto and A. Kocic, Phys. Rev. Lett. 60, 772 (1988).
8. B. Rosenstein, B. J. Warr and S. H. Park Phys. Rev. Lett. 62, 1433 (1989).
9. T. Appelquist, J. Terning and L. Wijewardhana Phys. Rev. Lett. 77, 1214 (1996).
10. M. Alford, K. Rajagopal and F. Wilczek, Phys. Lett. 422B, 247 (1998); R. Rapp, T. Schafer, E. Shuryak and M. Velkovski, Phys. Rev. Lett. 81, 53 (1998).
11. R. Pisarski and F. Wilczek, Phys. Rev. D 29, 338 (1984).
12. A. Kocic and J. Kogut, Phys. Rev. Lett. 74, 3109 (1995).
13. A. Kocic and J. Kogut, Nucl. Phys. B 455, 229 (1995).
14. J. Kogut, M. Stephanov and C. G. Strouthos Phys. Rev. D 58, 96001 (1998).
15. J. Kogut and D. Sinclair hep-lat/0005007.
16. S. Chandrasekharan and U.-J. Wiese, Phys. Rev. Lett. 83, 3116 (1999).
17. S. Chandrasekharan, Nucl. Phys. (Proc. Suppl.) B 63, 886 (1998).
18. H. G. Evertz, G. Lana and M. Marcu, Phys. Rev. Lett. 70, 875 (1993); U.-J. Wiese, Phys. Lett. 311B, 235 (1993).
19. S. Chandrasekharan, J. Cox, K. Holland and U.-J. Wiese, Nucl. Phys. B 576, 481 (2000).
20. J. Cox and K. Holland hep-lat/0003022.
21. L. Susskind, Phys. Rev. D 16, 3031 (1977).
22. S. Chandrasekharan, Chinese J. of Phys., Vol. 38, NO. 3-II 63 (2000) 696.
23. B. B. Beard and U.-J. Wiese, Phys. Rev. Lett. 77, 5130 (1996).
24. U.-J. Wiese, Phys. Lett. 311B, 235 (1993).
25. S. Chandrasekharan and J. C. Osborn, Computer Simulation Studies in Condensed Matter Physics, XIII, Eds. D. P. Landau, S. P. Lewis and H. B. Shuttler (Springer Verlag, Heidelberg, Berlin 2000).
26. J. C. Osborn, "Meron Cluster Updates with Binary Trees", in preparation.
27. V. Privman and M. E. Fisher, J. Stat. Phys. 33, (1983) 385; E. Brezin and J. Zinn-Justin, Nucl. Phys. B 257, 687 (1985).
28. M. Campostrini, A. Pelissetto, P. Rossi and E. Vicari, Phys. Rev. E 60, 3526 (1999).